nature physics

SUPPLEMENTARY INFORMATION

DOI: 10.1038/NPHYS2561

Quantum dynamics of a mobile spin impurity

Takeshi Fukuhara[1], Adrian Kantian[2], Manuel Endres[1], Marc Cheneau[1], Peter Schauß[1], Sebastian Hild[1], David Bellem[1], Ulrich Schollwöck[3], Thierry Giamarchi[2], Christian Gross[1], Immanuel Bloch[1,3], and Stefan Kuhr[1,4]

[1] *Max-Planck-Institut für Quantenoptik, 85748 Garching, Germany*
[2] *DPMC-MaNEP, University of Geneva, 24 Quai Ernest-Ansermet, 1211 Geneva, Switzerland*
[3] *Fakultät für Physik, Ludwig-Maximilians-Universität München, 80799 München, Germany*
[4] *University of Strathclyde, Department of Physics, SUPA, Glasgow G4 0NG, United Kingdom*

12th December 2012

Contents

DOI: 10.1038/NPHYS2561

1 The two-species Bose-Hubbard model and the Heisenberg model limit

We described the effective dynamics in a 1D lattice by a two-species single-band Bose-Hubbard model[1], which is valid at the temperatures, interaction strengths and lattice depths relevant to this study:

$$\hat{H}_{\mathrm{BH}} = -J \sum_{\langle j,k\rangle,\sigma} \hat{b}^{\dagger}_{\sigma,j}\hat{b}_{\sigma,k} + \sum_{j,\sigma,\sigma'} \frac{U}{2}\hat{n}_{\sigma,j}(\hat{n}_{\sigma',j} - \delta_{\sigma,\sigma'}) + \sum_{j,\sigma}(V_j^{\mathrm{trap}} - \mu)\hat{n}_{\sigma,j}. \tag{1}$$

Here, $\langle j,k\rangle, \sigma = \uparrow, \downarrow$ is the summation index comprising all neighboring sites j and k and the two bosonic species '$\uparrow$' and '$\downarrow$', J is the single-particle tunneling rate, and $\hat{b}^{\dagger}_{\sigma,j}$ ($\hat{b}_{\sigma,j}$) is the creation (annihilation) operator for a boson of type σ on lattice site j. The species-independent on-site interaction energy is denoted by U, whereas $\hat{n}_{\sigma,j}$ are the atomic number operators, $\delta_{\sigma,\sigma'}$ is the Kronecker symbol, and μ is the chemical potential. The external harmonic confinement with trapping frequency $\omega_{\mathrm{trap}}/2\pi$ is described by $V_j^{\mathrm{trap}} = \frac{1}{2}m\omega_{\mathrm{trap}}^2(ja_{\mathrm{lat}})^2$, where m is the mass of ^{87}Rb, and a_{lat} is the lattice constant.

In the limit of large interactions ($U \gg J$) and unity filling, it is possible to treat $\hat{H}_{\mathrm{BH}}$ in second order perturbation theory[2–5], mapping it to the isotropic spin-1/2 Heisenberg Hamiltonian [Eq. (1a)], by constructing effective spin-1/2 operators

$$\hat{S}^x_j = \frac{1}{2}\left(\hat{b}^{\dagger}_{\uparrow,j}\hat{b}_{\downarrow,j} + \hat{b}^{\dagger}_{\downarrow,j}\hat{b}_{\uparrow,j}\right) \tag{2a}$$

$$\hat{S}^y_j = \frac{1}{2i}\left(\hat{b}^{\dagger}_{\uparrow,j}\hat{b}_{\downarrow,j} - \hat{b}^{\dagger}_{\downarrow,j}\hat{b}_{\uparrow,j}\right) \tag{2b}$$

$$\hat{S}^z_j = \frac{1}{2}\left(\hat{n}_{\uparrow,j} - \hat{n}_{\downarrow,j}\right) \tag{2c}$$

and by introducing the exchange coupling $J_{\mathrm{ex}} = 4J^2/U$.

In principle, the parabolic confinement V_i makes the superexchange coupling site-dependent,

$$J_{\mathrm{ex},j} = \frac{4J^2U}{U^2 - (V_j - V_{j+1})^2}. \tag{3}$$

However, given the relatively small system size (12 sites) and low trapping frequency $\omega_{\mathrm{trap}}/2\pi = 85\,\mathrm{Hz}$, the variation of J_{ex} across the system does not exceed 2% at $V_x = 10\,E_r$. We can therefore safely consider the superexchange coupling constant, with $J_{\mathrm{ex},j} \approx J_{\mathrm{ex}} = 4J^2/U$.

2 Post-selecting samples

In order to visualize the role of our post-selection method, we plotted the probability distributions of empty sites obtained from negative images including chains with more than one empty site (Fig. S1). We observe a clear decrease of the signal contrast as the maximum number of empty sites becomes larger. Although this is partially due to the temperature (which we discuss in the main text for positive images), the main reason for the decrease is that we cannot distinguish between spin impurities and excitations within the negative image.

The post-selection relies on the assumption that there is exactly one spin impurity in the system. This assumption is not valid in the following two cases. First, the spin-flip on the initial site may fail due to the finite efficiency of the multi-site addressing scheme. In this case, if there is only one thermal excitation in the region of interest of the system, we count this excitation as the spin impurity. Second, if there is a hole at the addressed site, no spin impurity is introduced into the system and the hole is mistakenly detected as the impurity. A hole is moving much faster than the impurity and after averaging over samples of different system size its quantum interference disappears over the relatively longer time scales on which spin-wave dynamics occurs. In both cases, we obtain distributions of thermal excitations, which have no clear interference-like structure. What we obtained after post-selecting samples in our experiment is the sum of the position distribution of the spin impurity in the lower-temperature systems and the distribution of the thermal excitation. This leads to a decrease in contrast, which explains the small differences between the experimental data and the model in Fig. 2 of the main text.

Furthermore, this mechanism for the reduction in contrast is why we claim in the manuscript that the post-selected data should actually correspond to an even lower temperature (and thus higher contrast) than indicated in Fig. 3d of the main text. This remaining ambiguity of the spin-impurity position within the post-selected data could in principle be resolved by using direct spin-selective single-atom detection, which would allow for simultaneous imaging of both bath and impurity atoms. However, this is experimentally challenging.

DOI: 10.1038/NPHYS2561

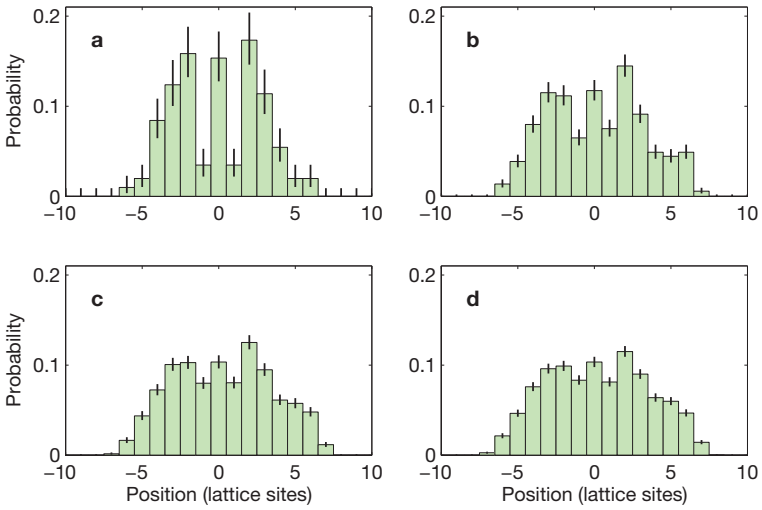

Supplementary Figure 1 | Post-selecting samples. Shown are position distribution of the single-spin impurity for $J/U = 0.053$ and a hold time of 60 ms, after post-selecting samples with one (**a**), less than three (**b**), four (**c**), and five (**d**) empty sites in the chain.

3 Temperature effects

We investigated the influence of temperature on the spin impurity dynamics for $J/U = 0.23$ ($V_x = 5\,E_r$), in addition to $J/U = 0.053$ ($V_x = 10\,E_r$) which was discussed in the main text. For this purpose, we numerically simulated the position distributions of the spin impurity after an evolution time of 4 ms for different temperatures (Fig. S2a). The simulation shows that even close to the transition point, the propagation velocity as a function of temperature remains constant whereas the contrast decreases (Fig. S2b and c), similar to the strongly interacting limit.

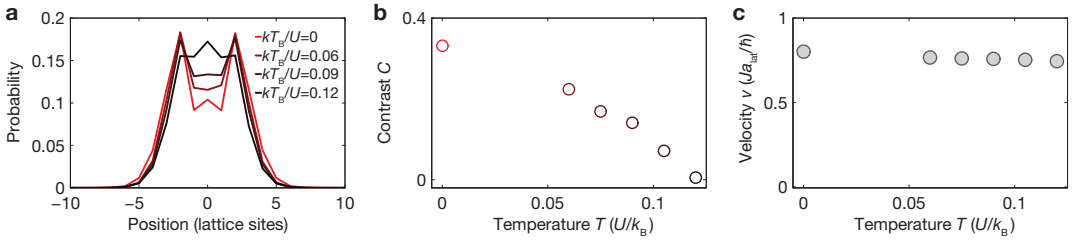

Supplementary Figure 2 | Effects of temperature on the dynamics. a Position distribution of the spin impurity for $J/U = 0.23$ and a hold time of 4 ms calculated with t-DMRG for different temperatures. Temperature dependence of the contrast (**b**) and the spreading velocity (**c**) extracted from the dataset of **a**.

4 Signatures of polaronic behaviour

We have measured the time evolution of the impurity distribution, $\langle \hat{n}_{\downarrow,j}(t) \rangle$, and demonstrated that these results can be fitted reasonably well by using the wave function of an independently evolving single particle for all values of J/U. We interpret this as spreading of the impurity inside the bath similar to a free particle with a renormalized tunneling amplitude (i.e., renormalized propagation velocity; see Fig. 4d in the main text). Our t-DMRG simulations further support this interpretation. Additional to matching the measured profiles at all values of J/U, the simulations show that the mean-square width of the impurity wave packet, $\sqrt{\sum_j j^2 \langle \hat{n}_{\downarrow,j}(t) \rangle}$, increases linearly with time (not shown).

This ballistic motion of the impurity with renormalized tunneling can be seen as a first hint of polaronic behaviour. As the impurity propagates, its repulsive interaction with the bath continuously displaces '$\uparrow$'-atoms around it, creating an area of decreased bath density that moves with the impurity. We have analysed the displacement of the bath atoms by the propagating impurity in detail for the case $J/U = 0.47$ (Fig. 5 in the main text). As an addition to this, our analysis shows that the time-dependent density of the impurity on a given site evolves opposite to the density of the bath atoms on the same site (Fig. S3a) and shows good agreement with our t-DMRG simulations. These simulations also show that the time-dependence of the correlation-hole depth on site j, defined as $\mathcal{N}_{\downarrow\uparrow}(j,j+1) - \mathcal{N}_{\downarrow\uparrow}(j,j)$, evolves in the same way as the impurity density on the same site (see Figs. S3a and b). Our experimental setup does not permit a direct measurement of the anti-correlation moving with the impurity. However, the measurement of the similar but opposite behaviour of the on-site parity between impurity and bath atoms, and their good agreement with simulations, provides indirect, but strong evidence that, in our system, the spin impurity forms a polaronic excitation in the SF regime.

DOI: 10.1038/NPHYS2561

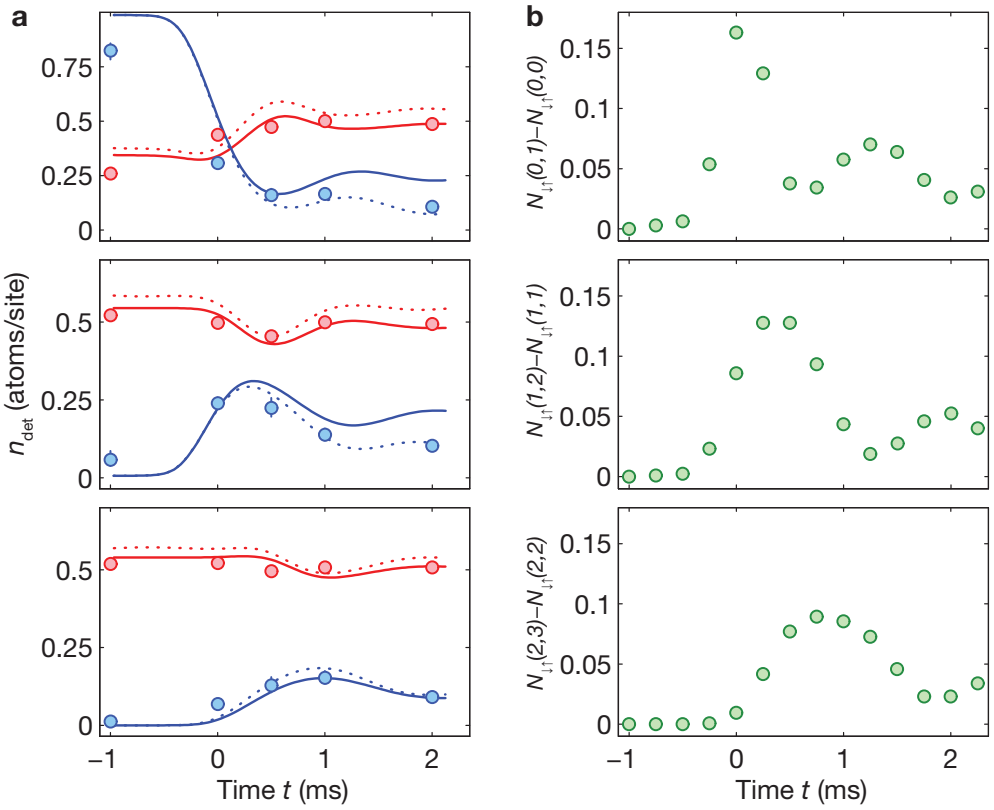

Supplementary Figure 3 | Time evolution of the impurity and bath densities and of the correlation-hole depth. a Measured density of the impurity (blue circles) and the parity-projected density of the bath (red circles) at the centre site ($j = 0$, upper panel), at one ($j = 1$, center panel) and two sites ($j = 2$, lower panel) away from the centre. The impurity is released from the pinning beam at $t = 0$. The lines show corresponding numerical simulations with temperature and chemical potential chosen to reproduce the initial atom distribution in the MI regime (solid lines) and with zero temperature and a fixed bath atom number of 13 (dashed line). Almost all statistical error bars are smaller than the circles. **b** Simulated time-evolution of the correlation-hole depths on sites $j = 0, 1, 2$, evolving in the same way as the impurity density on the same site.

References

1. Cazalilla, M., Citro, R., Giamarchi, T., Orignac, E. & Rigol, M. One dimensional bosons: From condensed matter systems to ultracold gases. *Rev. Mod. Phys.* **83,** 1405–1466 (2011).
2. Kuklov, A. & Svistunov, B. Counterflow superfluidity of two-species ultracold atoms in a commensurate optical lattice. *Phys. Rev. Lett.* **90,** 100401 (2003).
3. Duan, L.-M., Demler, E. & Lukin, M. Controlling Spin Exchange Interactions of Ultracold Atoms in Optical Lattices. *Phys. Rev. Lett.* **91,** 090402 (2003).
4. García-Ripoll, J. J. & Cirac, J. I. Spin dynamics for bosons in an optical lattice. *New J. Phys.* **5,** 76 (2003).
5. Altman, E., Hofstetter, W., Demler, E. & Lukin, M. D. Phase diagram of two-component bosons on an optical lattice. *New J. Phys.* **5,** 113 (2003).